

Giant electrocaloric effect at the antiferroelectric-to-ferroelectric phase boundary in $\text{Pb}(\text{Zr}_x\text{Ti}_{1-x})\text{O}_3$ ^{EP}

Cite as: Appl. Phys. Lett. **115**, 023902 (2019); <https://doi.org/10.1063/1.5096592>
 Submitted: 19 March 2019 . Accepted: 20 June 2019 . Published Online: 10 July 2019

A. V. Kimmel, O. T. Gindele , D. M. Duffy , and R. E. Cohen 

COLLECTIONS

 This paper was selected as an Editor's Pick



View Online



Export Citation



CrossMark

ARTICLES YOU MAY BE INTERESTED IN

[Antenna-coupled spintronic terahertz emitters driven by a 1550 nm femtosecond laser oscillator](#)

Applied Physics Letters **115**, 022405 (2019); <https://doi.org/10.1063/1.5089421>

[Aberration-corrected cryogenic objective mirror with a 0.93 numerical aperture](#)

Applied Physics Letters **115**, 033701 (2019); <https://doi.org/10.1063/1.5110546>

[Strain effect on thermoelectric properties of SrRuO₃ epitaxial thin films](#)

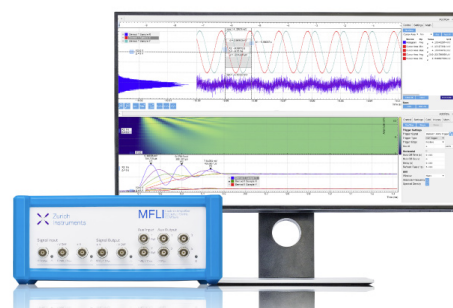
Applied Physics Letters **115**, 022403 (2019); <https://doi.org/10.1063/1.5097927>

Challenge us.

What are your needs for periodic signal detection?



Zurich
Instruments



Giant electrocaloric effect at the antiferroelectric-to-ferroelectric phase boundary in $\text{Pb}(\text{Zr}_x\text{Ti}_{1-x})\text{O}_3$

Cite as: Appl. Phys. Lett. **115**, 023902 (2019); doi: [10.1063/1.5096592](https://doi.org/10.1063/1.5096592)

Submitted: 19 March 2019 · Accepted: 20 June 2019 ·

Published Online: 10 July 2019



View Online



Export Citation



CrossMark

A. V. Kimmel,^{1,2,a)} O. T. Gindele,²  D. M. Duffy,²  and R. E. Cohen^{2,3,4} 

AFFILIATIONS

¹CIC nanoGUNE, Tolosa Hiribidea, 76, San Sebastian 20018, Spain

²Department of Physics and Astronomy, University College London, Gower Street, London WC1E 6BT, United Kingdom

³Extreme Materials Initiative, Geophysical Laboratory, Carnegie Institution for Science, Washington, DC 20015, USA

⁴Department of Earth and Environmental Sciences, Ludwig-Maximilians Universität München, Theresienstr. 41 80333 Munich, Germany

^{a)} Author to whom correspondence should be addressed: a.kimmel@nanogune.eu

ABSTRACT

Molecular dynamics simulations predict a giant electrocaloric effect at the ferroelectric-antiferroelectric phase boundary in PZT (PbTiO_3 - PbZrO_3). These large-scale simulations also give insights into the atomistic mechanisms of the electrocaloric effect in $\text{Pb}(\text{Zr}_x\text{Ti}_{1-x})\text{O}_3$. We predict a positive electrocaloric effect in ferroelectric PZT, but antiferroelectric PZT exhibits a negative-to-positive crossover with the increasing temperature or electric field. At the antiferroelectric-to-ferroelectric phase boundary, we find complex domain patterns. We demonstrate that the origin of the giant electrocaloric change of temperature is related to the easy structural response of the dipolar system to external stimuli in the transition region.

Published under license by AIP Publishing. <https://doi.org/10.1063/1.5096592>

The electrocaloric effect is a reversible temperature change (ΔT) in materials under adiabatic conditions in response to the applied electric (or magnetic) field. The discovery of a giant 12 K electrocaloric effect (ECE) in thin films of Zr-rich lead titanate compositions fueled interest into the development of novel ferroelectric-based ECE materials.¹

Giant and moderate ECEs have since been reported for classical ferroelectrics (FEs) like BaTiO_3 ² and for several relaxor materials.³ $\text{Pb}(\text{Zr}_{1-x}\text{Ti}_x)\text{O}_3$ (PZT) is a disordered solid solution ABO_3 perovskite, with Pb atoms occupying the A-site and Ti and Zr cations randomly arranged among the B-sites. PbTiO_3 (PTO), the $x=0.0$ end member of $\text{Pb}(\text{Zr}_x\text{Ti}_{1-x})\text{O}_3$, is a classical ferroelectric (FE), and the other end member PbZrO_3 (PZO) ($x=1.0$) is an antiferroelectric (AFE). Near $x=0.95$, there is a phase boundary that separates AFE and FE phases.⁴ $\text{Pb}(\text{Zr}_{1-x}\text{Ti}_x)\text{O}_3$ (PZT) remains an active area of research for novel ECE materials.^{5,6} The response of PZT to the applied electric field in the transition region between its ferroelectric and antiferroelectric phases is of particular interest since a giant electrocaloric response has been found experimentally for compositions close to this region.¹ Studies of the electrocaloric response of AFE $\text{Pb}_{0.97}\text{La}_{0.02}(\text{Zr}_{0.95}\text{Ti}_{0.05})\text{O}_3$ have provided an insight into a mechanism for the negative electrocaloric response. The authors suggested that the misalignment of noncollinear

dipoles provides different entropy contributions depending on the direction of the applied electric field.⁷

Several theoretical works discuss caloric effects in perovskites. Large electrocaloric effects have been observed in the vicinity of ferroelectric-paraelectric phase transitions; however, little is known about the ECE near the AFE-FE phase boundary. Recent work with effective Hamiltonians reveals a strong potential of electrocalorics for thin PZO films with FE and AFE phase competition.⁸ Phenomenological modeling for an AFE system predicted the negative electrocaloric effect in PZO ceramics, which agrees well with direct measurements of the electrocaloric temperature change (EC ΔT) in this system.⁹

Molecular dynamics (MD) methods, using shell model potentials fit to first principles calculations, are promising models for computing the thermal behavior of materials, since they do not require assumptions about the important degrees of freedom. Such models have been used to study the ECE in LiNbO_3 , PMN-PT, and BaTiO_3 .¹⁰⁻¹² These simulations provide insight into the universal principles related to optimal operating temperatures for the electrocaloric effect.

In this work, we studied the effects of the composition on electrocaloric properties of PZT using large scale MD simulations with first-principles based shell model potentials.¹³ We modeled a wide

range of ferroelectric and antiferroelectric compositions of $\text{Pb}(\text{Zr}_x\text{Ti}_{1-x})\text{O}_3$. We found that the electrocaloric response of PZT correlates with the type of ferroelectric order and that a giant electrocaloric response exists at the phase boundary of PZT, where antiferroelectric and ferroelectric orders coexist.

To model the electrocaloric properties of PZT, we use a core-shell force field, which includes all degrees of freedom. This *ab initio* based interatomic potential reproduces a set of temperature and composition induced phase transitions characteristic of $\text{Pb}(\text{Zr}_x\text{Ti}_{1-x})\text{O}_3$.¹³ The potential model underestimates the Curie temperatures with respect to experiment for PbTiO_3 [600 K vs 750 K (Ref. 4)] and PbZrO_3 [400 K vs 507 K (Ref. 9)], which is a reasonable error for this type of force field.

A set of $\text{Pb}(\text{Zr}_x\text{Ti}_{1-x})\text{O}_3$ compositions were modeled using the DL_POLY code.¹⁴ We study AFE and FE compositions with x equal to 0.5, 0.9, and 1 (corresponding to AFE PbZrO_3), together with $x = 0$ (corresponding to FE PbTiO_3), 0.7, 0.8, 0.85, and 0.95 shown in the [supplementary material](#). The B-site cations, Ti and Zr, were randomly distributed over the B-sites. We use the adiabatic shell model (also known as the dynamical model¹⁵) to incorporate polarisability into molecular dynamics simulations with the shell masses equal to 3.5%, 8.3%, 17.12%, and 12.5% of the atomic mass of Pb, Ti, Zr, and O, respectively. We used relatively large $20 \times 20 \times 20$ supercells (80 000 core and shell particles). Each composition was equilibrated at 100 K for 40 ps, followed by the application of an electric field along the polar axis. The direction of the polar axis depends on the composition of $\text{Pb}(\text{Zr}_x\text{Ti}_{1-x})\text{O}_3$ and was taken as [001] for PZO, [111] for the Zr content from 0.95 to 0.50, and [001] for $x \geq 0.4$. The strength of the applied electric field was 0, 5, 10, 15, 20, 25, 50, 75, and 100 MV/m. We used a 0.2 fs time step and constant average temperature and stress (with the latter average always set to zero), so-called, $N\sigma T$ ensemble with the Nosé-Hoover thermostat (0.01 ps) and barostat (0.5 ps) for equilibration of individual systems during 8 ps. The equilibration was followed by a 12 ps production run over which the polarization value was calculated.

To study the electrocaloric effect, we used the indirect method, where the change of temperatures was calculated from the Maxwell related expression

$$\Delta T = - \int_0^E \frac{TV}{C_{p,E}} \left(\frac{\partial P}{\partial T} \right)_E dE. \quad (1)$$

Here, E is the applied electric field, T is the temperature, V is the volume of the simulation cell, and $C_{p,E}$ is the heat capacity per cell under constant electric field and pressure. We calculate the ECE change of temperature (ΔT), by integrating equation (1) numerically. The values of $C_{p,E}$ were calculated as the derivative of the total energy with temperature ($\frac{\partial E_{\text{tot}}}{\partial T}$) at a given value of electric field, E , and are in agreement with experiment¹⁶ (see the [supplementary material](#)).

The temperature and field dependence of the electrocaloric change in temperature, ΔT , were calculated for FE PTO via expression Eq. (1) [see [supplementary material](#), Fig. 1(a)]. A characteristic dominant peak at 650 K (the PTO Curie temperature reproduced by our force field) moves toward higher temperatures for larger applied electric fields, typical for ferroelectrics.¹⁰ The magnitude of the electrocaloric effect calculated for PTO is in good agreement with similar method computations for LiNbO_3 which gives 17 K at an applied field of 50 MV/m vs 16 K in our computations for PTO.¹⁰

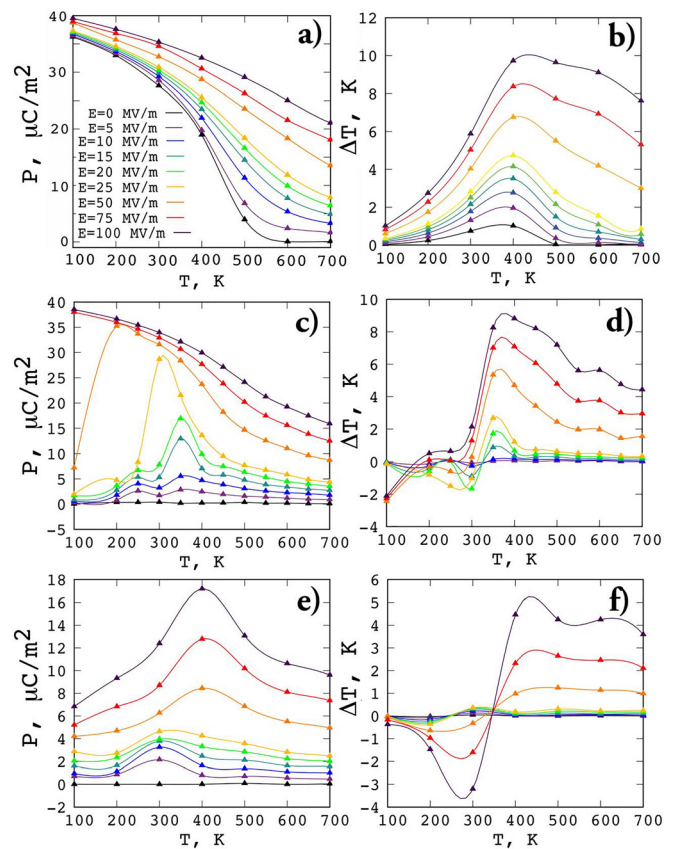


FIG. 1. Polarization and EC temperature change with temperature and different applied electric fields for (a) and (b) $\text{Pb}_{0.70.5}\text{Ti}_{0.5}\text{O}_3$, (c) and (d) $\text{Pb}_{0.9}\text{Ti}_{0.1}\text{O}_3$, and (e) and (f) PbZrO_3 .

The morphotropic phase boundary (MPB) is found in a narrow compositional range around $x = 0.5$, where the FE phase with rhombohedral symmetry transforms to the tetragonal phase. It is now known that there is a monoclinic transition region between the rhombohedral and tetragonal phases.¹⁷ We found that the electrocaloric effect in FE $\text{Pb}(\text{Zr}_x\text{Ti}_{1-x})\text{O}_3$ with $x = 0.5$ and 0.7 exhibits very similar behavior. The peaks of ΔT broaden, which reflects the B-site cation disorder and reduction of the correlation length in the material¹⁸ [see Figs. 1(a) and 1(b) and [supplementary material](#), Figs. 1(b) and 1(c)]. The ΔT curves peak above T_c with the increasing electric field [Fig. 1(b)], similar to what was computed for LiNbO_3 .¹⁰

The transition boundary between AFE and FE phases in $\text{Pb}(\text{Zr}_x\text{Ti}_{1-x})\text{O}_3$ has been shown to exist within a composition region around $x = 0.95\text{--}0.9$.⁴ It is challenging to identify the precise composition of the transition region between AFE and FE phases experimentally, due to the purity of the samples, composition variance, especially for solid solution materials, and the presence of surface effects that may stabilize the FE phase. The force field used in this work is able to reproduce the composition induced AFE-FE phase boundary, but the model gives a boundary wider than seen experimentally—we find that composites with $x > 0.8$ exhibit antiferroelectric properties.¹³ Furthermore, we have performed calculations of the electrocaloric

properties for several of the AFE PZT compositions with x of 0.9 and 1 (PbZrO_3), while the results for 0.85 and 0.95 are given in the [supplementary material](#).

We found that the electrocaloric response of AFEs is very different from that of the FE systems. In AFEs, the applied electric field causes T_c to decrease [Figs. 1(c)–1(f) and [supplementary material](#), Fig. 2], whereas ferroelectric materials show the opposite tendency. A common feature of all studied AFE PZT is a negative-to-positive crossover that varies with the temperature and composition. Positive values of the EC ΔT are related to the reduction of isothermal entropy. In classical FEs, these are related to the drop of macroscopic polarization with increasing temperature. However, in AFEs, the polarization may exhibit an opposite behavior, i.e., increasing with increasing temperature under the applied field. This occurs simply because the applied field favors net polarization, and consequently, dielectric susceptibility increases with temperature. The latter results in a negative change of isothermal entropy and the reverse electrocaloric effect (see the [supplementary material](#)).

PZO does not exhibit a macroscopic polarization at zero field, as expected for an AFE. The applied electric field induces a polarization that increases up to the critical temperature, T_c , and then falls with a further temperature increase [see Figs. 1(e) and 1(f)]. However, the induced polar state of PZO at an applied field of 100 MV/m is only $18 \mu\text{C}/\text{m}^2$, which is 40% lower than that of PTO. Ferroelectrics can also show negative ECE originating from polarization rotation, where the polarization along the field direction increases with temperature due to the approaching phase transition.^{11,12} Calculated behavior of ΔT for PZO exhibits a crossover from negative to positive values in the vicinity of T_c as shown in Fig. 1(f). For applied electric fields $< 50 \text{ MV}/\text{m}$, the EC change in temperature is negative below T_c (at

$T = 250 \text{ K}$, the value of EC ΔT is -0.7 K with an applied field of $25 \text{ MV}/\text{m}$).

At zero applied field, AFE PZT ($x = 0.95, 0.9, 0.85$, and 0.8) shows zero macroscopic polarization, but local dipoles, as will be shown later, form competing AFE and FE domains. The application of an electric field enhances the polarization, which reaches its maximum at temperatures of 400 K, 350 K, and 300 K characteristic of each composition with $x = 0.85, 0.90$, and 0.95 , respectively [Figs. 1(c) and 1(d) and [supplementary material](#), Figs. 2(b)–2(d)].

The electrocaloric response of the studied AFEs is characterized by the negative-to-positive crossover. In PZO, the EC ΔT changes its sign once, whereas AFE PZT exhibits more complex EC behavior.

We have found that, in general, the ECE in FE and AFE $\text{Pb}(\text{Zr}_x\text{Ti}_{1-x})\text{O}_3$ with $x > 0$ is smaller compared to that in the pure FE PTO [22.01 K at $100 \text{ MV}/\text{m}$ of applied field [see [supplementary material](#), Fig. 2(a)]], but at lower temperatures and, thus, more usable under ordinary conditions. At the AFE-FE boundary, an enhanced caloric response is observed comparable to MPB PZT. The smallest EC response is observed in the pure AFE PZO of about 5 K at $100 \text{ MV}/\text{m}$ of applied field. The AFE PZT with $x = 0.8$ exhibits the EC ΔT of 6.1 K at a similar field (see [supplementary material](#), Fig. 1). Meanwhile, PZT with $x = 0.95$ and 0.9 exhibits values of EC ΔT of about 10 K ([supplementary material](#), Fig. 2), which is comparable with the EC response of MPB PZT at similar stimuli.

To understand the origin of the giant ECE and negative-to-positive crossover at the AFE-FE phase boundary, we analyzed the evolution of local dipoles in response to applied fields. We found that an AFE system may adopt complex dipole arrangements with a variety of possible states, such as dipole FE order, dipole disorder, and various AFE dipole arrangements characterized by zero macroscopic polarization.

In particular, at small applied fields and low temperatures, the AFE $\text{PbZr}_{0.95}\text{Ti}_{0.05}\text{O}_3$ exhibits a dynamically stable 2×1 pattern [Fig. 2(a)]. Here, the local dipoles are arranged as antiparallel double pairs along the X cartesian direction and single antiparallel arrangement along the Z axis [see directing arrows in the inset of Fig. 2(a)]. At higher temperatures, the order of local dipoles changes to a 1×1 pattern, where single antiparallel dipoles are alternating with the sites of dipole disorder [Fig. 2(b)]. Increasing the applied field to the critical value of $25 \text{ MV}/\text{m}$ leads to the rotation of local dipoles, and so the system turns into an induced polar FE state.

Increasing the Ti content leads to stabilization of a zig-zag pattern of AFE local dipoles [Fig. 2(c)]. Here, the local dipoles are arranged into antiparallel pairs. As the field increases, the system develops competing AFE and FE domains, with widths which correlate with the strength of the applied field. The critical field of $50 \text{ MV}/\text{m}$ switches the system to an induced polar FE monodomain state.

A higher Ti content in $\text{PbZr}_{0.85}\text{Ti}_{0.15}\text{O}_3$ increases the correlation length of the material,¹⁸ which leads to the formation of stripe ordering, with AFE dipole arrangement alternating with FE stripes [Fig. 2(d)].

We suggest that the nature of the giant EC ΔT in AFE PZT is related to the formation of competing AFE and induced FE orders that respond easily to applied fields and temperature. In ferroelectrics, the configurational entropy is related to the order maintained by a dipolar system. In the absence of the applied field, the change of polarization with temperature, $\frac{\partial P}{\partial T}$, is relatively small, except in the vicinity of the critical temperature, where this value is large. Thus, the

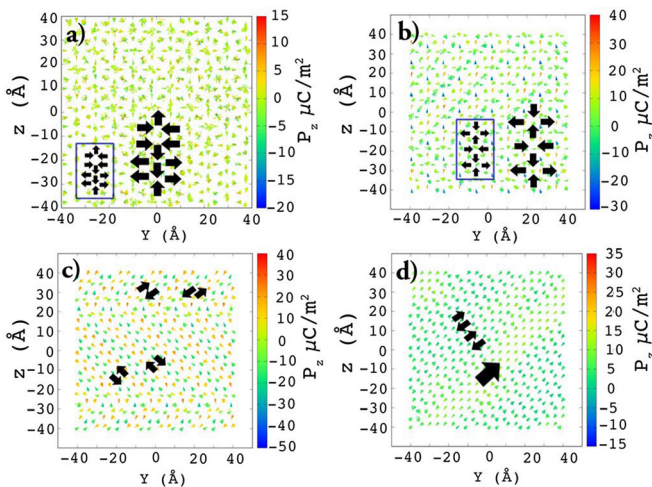


FIG. 2. Gradient color plot of projected local dipoles on the XZ plane: (a) AFE pattern in $\text{PbZr}_{0.95}\text{Ti}_{0.05}\text{O}_3$ at $T = 100 \text{ K}$ and zero field. The selected area exhibits a 2×1 pattern of local dipole arrangement as shown in an enlarged scheme with black arrows; (b) AFE pattern in $\text{PbZr}_{0.95}\text{Ti}_{0.05}\text{O}_3$ at $T = 300 \text{ K}$ and applied $E = 5 \text{ MV}/\text{m}$. The selected area exhibits 1×1 arrangement of local dipoles; (c) zig-zag-like AFE local dipole arrangement in $\text{PbZr}_{0.9}\text{Ti}_{0.1}\text{O}_3$ at $T = 100 \text{ K}$ at zero field; (d) stripe AFE-FE local dipole arrangement in $\text{PbZr}_{0.85}\text{Ti}_{0.15}\text{O}_3$ at 100 K and $E = 5 \text{ MV}/\text{m}$.

maximum of EC ΔT in ferroelectrics occurs when the system switches from FE to PE.

An AFE system may adopt complex configurations with a variety of possible dipole states—as dipole FE order, dipole disorder, and various AFE dipole arrangements with zero macroscopic polarization (as shown in Fig. 2, where the system maintained 2×1 and 1×1 patterns). We suggest that in AFE systems, the change from AFE to FE order occurs via a sequence of local minima with a partially preserved AFE order and the formation of competing AFE and FE domains.

We assume that with applied field, the aligned dipole configurations may become more advantageous to antipolar configurations. This leads to destabilization of antialigned arrangements of local dipoles in an AFE material leading to their partial or complete alignment and, consequently, formation of competing antiferroelectric and induced ferroelectric domains. The transition process may occur through initial canting as proposed in Ref. 7 and follows complete rotation similar to the mechanism proposed for FEs in Ref. 12.

In bulk PZO, the change of polarization, $\frac{\delta P}{\delta T}$, is relatively small (supplementary material, Fig. 2) because our system is free of defects, grain boundaries, and electrode contacts. Thus, each local dipole has to overcome a barrier for rotation. However, in AFE $\text{Pb}(\text{Zr}_x\text{Ti}_{1-x})\text{O}_3$, the presence of different types of B-site cations increases the configurational entropy of the system and supports multiple domain configurations. The Ti sites act as nucleation centers for the FE phase, facilitating the fast response of local dipoles to applied electric fields. At the AFE-FE phase boundary, the concentration of Ti centers is such that there are no FE ordered regions in the absence of an applied electric field; however, the application of an external electric field gives rise to FE ordering, which competes with the AFE order [Fig. 3(d)]. The maximum of EC ΔT in AFE composites occurs when the system switches to an induced polar FE monodomain.

We have studied the electrocaloric effect in PZT using molecular dynamics simulations with shell model force fields. Our results show giant electrocaloric effects for FE PTO, in good agreement with similar calculations performed for FE LiNbO_3 .¹⁰ We found a crossover from the negative to positive EC temperature change for all studied AFE PZT. The crossover temperatures correlate with the composition, which we believe to be related to the correlation length increase in the material.¹⁸ We have found that compositions close to the AFE-FE boundary of PZT exhibit an enhanced caloric response, comparable to that of MPB PZT, but with the maximum EC ΔT occurring at temperatures closer to ambient temperatures. Our methodology allows us to investigate the details of the polarization response at an atomistic level. Close to the AFE-FE boundary, we identified complex dipole configurations, with competing FE and AFE domain patterns. We postulate that the small energy barriers associated with growing/reducing these domains are responsible for the easy response of the polarization to the applied field and temperature and, hence, for the enhanced caloric response. Despite the high EC response, the critical temperature in many ferroelectric materials is considerably higher than room temperature, which substantially limits the potential for applications in solid-state devices. We have found that AFE PZT exhibits extrema of EC ΔT close to room temperature, in the range of 300–400 K. In addition, solid solution $\text{Pb}(\text{Zr}_x\text{Ti}_{1-x})\text{O}_3$ offers great variability in critical temperatures and in ECE magnitude, which allows for compositional engineering of materials for electrocaloric applications. In summary,

our findings suggest pathways for tuning the operating temperatures of ECE devices and find solutions for a broad range of operating conditions.

See the [supplementary material](#) for the calculated heat capacity and isothermal change of entropy in AFE and FE $\text{Pb}(\text{Zr}_x\text{Ti}_{1-x})\text{O}_3$. We also calculated the electrocaloric effect in FE PbTiO_3 and FE $\text{PbZr}_{0.7}\text{Ti}_{0.3}\text{O}_3$, together with polarization and the electrocaloric temperature change in AFE $\text{PbZr}_{0.95}\text{Ti}_{0.05}\text{O}_3$ and AFE $\text{PbZr}_{0.85}\text{Ti}_{0.15}\text{O}_3$.

The authors acknowledge UCL computational facilities LEGION and MYRIAD. A.K. was supported by the European Union's Horizon 2020 research and innovation programme under the Marie Skłodowska-Curie Grant Agreement No. 796781. R.E.C. was supported by the U. S. Office of Naval Research Grant Nos. N00014-12-1-1038, N00014-14-1-0516, and N00014-17-1-2768, the Carnegie Institution for Science, and the European Research Council Advanced Grant ToMcCaT.

REFERENCES

- A. S. Mischenko, Q. Zhang, J. F. Scott, R. W. Whatmore, and N. D. Mathur, "Giant electrocaloric effect in thin-film PZT," *Science* **311**, 1270–1271 (2006); e-print [arXiv:0511487](#).
- S. Kar-Narayan and N. D. Mathur, "Direct and indirect electrocaloric measurements using multilayer capacitors," *J. Phys. D: Appl. Phys.* **43**, 032002 (2010); e-print [arXiv:0912.1978](#).
- S. G. Lu, B. Rožič, Q. M. Zhang, Z. Kutnjak, X. Li, E. Furman, L. J. Gorny, M. Lin, B. Malič, M. Kosec, R. Blinc, and R. Pirc, "Organic and inorganic relaxor ferroelectrics with giant electrocaloric effect," *Appl. Phys. Lett.* **97**(16), 162904 (2010).
- D. I. Woodward, J. Knudsen, and I. M. Reaney, "Review of crystal and domain structures in the PZT solid solution," *Phys. Rev. B* **72**, 104110 (2005).
- T. Zhang, W. Li, Y.-F. Hou, Y. Yu, W. P. Cao, Y. Feng, and W. Fei, "Positive/negative electrocaloric effect induced by defect dipoles in PZT ferroelectric bilayer thin films," *R. Soc. Chem. Adv.* **6**, 71934–71939 (2016).
- Z. Zuo, B. Chen, B. Wang, H. Yang, Q. Zhan, Y. Liu, J. Wang, and R.-W. Li, "Strain assisted electrocaloric effect in $\text{Pb}(\text{Zr}_{0.95}\text{Ti}_{0.05})\text{O}_3$ films on $0.7\text{Pb}(\text{Mg}_{1/3}\text{Nb}_{2/3})\text{O}_3$ - 0.3PbTiO_3 substrate," *Sci. Rep.* **5**, 16164 (2015).
- W. Geng, X. M. Y. Liu, L. Bellaiche, J. F. Scott, B. Dkhil, and A. Jiang, "Giant negative electrocaloric effect in antiferroelectric La-doped $\text{Pb}(\text{ZrTi})\text{O}_3$ thin films near room temperature," *Adv. Mater.* **27**(20), 3165 (2015).
- M. Kingsland, S. Lisenkov, and I. Ponomareva, "Unveiling electrocaloric potential of antiferroelectrics with phase competition," *Adv. Theory Simul.* **1**, 1800096 (2018).
- R. Pirc, B. Rožič, J. Koruza, B. Malič, and Z. Kutnjak, "Negative electrocaloric effect in antiferroelectric PbZrO_3 ," *Europhys. Lett.* **107**, 17002 (2014).
- M. C. Rose and R. E. Cohen, "Giant electrocaloric effect around T_c ," *Phys. Rev. Lett.* **109**, 187604 (2012); M. Rose and R. E. Cohen, "Erratum: Giant electrocaloric effect around T_c ," *ibid.* **112**, 249901 (2014).
- H. H. Wu and R. E. Cohen, "Electric-field-induced phase transition and electrocaloric effect in PMN-PT," *Phys. Rev. B* **96**, 054116 (2017).
- H. H. Wu and R. E. Cohen, "Polarization rotation and the electrocaloric effect in barium titanate," *J. Phys.: Condens. Matter* **29**, 485704 (2017).
- O. Gindele, A. Kimmel, M. G. Cain, and D. Duffy, "Shell model force field for lead zirconate titanate $\text{Pb}(\text{Zr}_{1-x}\text{Ti}_x)\text{O}_3$," *J. Phys. Chem. C* **119**, 17784–17789 (2015).
- I. T. Todorov, W. Smith, K. Trachenko, and M. T. Dove, "DL-POLY_3: New dimensions in molecular dynamics simulations via massive parallelism," *J. Mater. Chem.* **16**, 1911 (2006).
- D. Fincham and P. J. Mitchell, "Shell model simulations by adiabatic dynamics," *J. Phys.: Condens. Matter* **5**, 1031 (1993).
- K. Morimoto, A. Uematsu, S. Sawai, K. Hisano, and T. Yamamoto, "Simultaneous measurement of thermophysical properties and dielectric

- properties of PZT-based ferroelectric ceramics by thermal radiation calorimetry," *Int. J. Thermophys.* **24**, 3 (2003).
- ¹⁷B. Noheda, D. E. Cox, G. Shirane, J. A. Gonzalo, L. E. Cross, and S.-E. Park, "A monoclinic ferroelectric phase in the $\text{Pb}(\text{Zr}_{(1-x)}\text{Ti}_x)\text{O}_3$ solid solution," *Appl. Phys. Lett.* **74**, 2059 (1999); e-print [arXiv:9903007](https://arxiv.org/abs/9903007); R. E. Cohen, "Morphing into action," *Nature* **562**, 48–49 (2018); N. Zhang, H. Yokota, A. M. Glazer, Z. Ren, D. Keen, D. S. A. Keeble, P. A. Thomas, and Z.-G. Ye, "The missing boundary in the phase diagram of PbZrTiO_3 ," *Nat. Commun.* **5**, 5231 (2014); A. Bogdanov, A. Mysovsky, C. J. Pickard, and A. V. Kimmel, "Modelling the structure of Zr-rich PZT by a multiphase approach," *Phys. Chem. Chem. Phys.* **18**, 28316 (2016); H. Fu and R. E. Cohen, "Polarization rotation mechanism for ultrahigh electromechanical response in single-crystal piezoelectrics," *Nature* **403**, 281–283 (2000); M. Ahart, M. Somayazulu, R. E. Cohen, P. Ganesh, P. Dera, H. K. Mao, R. J. Hemley, Y. Ren, P. Liermann, and Z. Wu, "Origin of morphotropic phase boundaries in ferroelectrics," *ibid.* **451**, 545 (2008).
- ¹⁸G. G. Guzman-Verri and P. B. Littlewood, "Why is the electrocaloric effect so small in ferroelectrics?," *APL Mater.* **4**, 064106 (2016).